BBA - Biomembranes 1863 (2021) 183449

Contents lists available at ScienceDirect

BBA - Biomembranes

journal homepage: www.elsevier.com/locate/bbamem

Membrane interactions of the anuran antimicrobial peptide HSP1-NH_2: Different aspects of the association to anionic and zwitterionic biomimetic systems

Isabela P. Gomes[a], Talita L. Santos[a], Amanda N. de Souza[a], Lúcio O. Nunes[a], Gabriele A. Cardoso[a,b], Carolina O. Matos[c], Lívia M.F. Costa[a], Luciano M. Lião[c], Jarbas M. Resende[b], Rodrigo M. Verly[a,*]

[a] Departamento de Química – Universidade Federal dos Vales do Jequitinhonha e Mucuri, 39100-000 Diamantina, MG, Brazil
[b] Departamento de Química – Universidade Federal de Minas Gerais, P.O. Box 486, 31270-901 Belo Horizonte, MG, Brazil
[c] Instituto de Química – Universidade Federal de Goiás, 74690-900 Goiânia, GO, Brazil

ARTICLE INFO

Keywords:
Peptide-membrane interaction
Antimicrobial peptides
Antimicrobial mechanism of action
Conformational analysis of peptides
Membrane active peptides
Biophysical prediction of peptide-membrane interactions
Membrane-dependent composition

ABSTRACT

Studies have suggested that antimicrobial peptides act by different mechanisms, such as micellisation, self-assembly of nanostructures and pore formation on the membrane surface. This work presents an extensive investigation of the membrane interactions of the 14 amino-acid antimicrobial peptide hylaseptin P1-NH_2 (HSP1-NH_2), derived from the tree-frog *Hyla punctata*, which has stronger antifungal than antibacterial potential. Biophysical and structural analyses were performed and the correlated results were used to describe in detail the interactions of HSP1-NH_2 with zwitterionic and anionic detergent micelles and phospholipid vesicles. HSP1-NH_2 presents similar well-defined helical conformations in both zwitterionic and anionic micelles, although NMR spectroscopy revealed important structural differences in the peptide N-terminus. ^2H exchange experiments of HSP1-NH_2 indicated the insertion of the most N-terminal residues (1–3) in the DPC-d_{38} micelles. A higher enthalpic contribution was verified for the interaction of the peptide with anionic vesicles in comparison with zwitterionic vesicles. The pore formation ability of HSP1-NH_2 (examined by dye release assays) and its effect on the size and surface charge as well as on the lipid acyl chain ordering (evaluated by Fourier-transform infrared spectroscopy) of anionic phospholipid vesicles showed membrane disruption even at low peptide-to-phospholipid ratios, and the effect increases proportionately to the peptide concentration. On the other hand, these biophysical investigations showed that a critical peptide-to-phospholipid ratio around 0.6 is essential for promoting disruption of zwitterionic membranes. In conclusion, this study demonstrates that the binding process of the antimicrobial HSP1-NH_2 peptide depends on the membrane composition and peptide concentration.

1. Introduction

At a time of increasing microbial resistance, antimicrobial peptides (AMPs) provide an interesting alternative to conventional antibiotics [1]. The majority of AMPs are cationic, and their microbicide action is intrinsically related to their interaction with microorganism membranes, which is driven by electrostatic and hydrophobic forces [2,3]. In addition, it is widely reported that most cationic AMPs also adopt well-defined structures when interacting with phospholipid membranes that distribute amino acid residues in an amphipathic arrangement [3]. The degree of amphipathicity can be evaluated by the relative proportion of hydrophilic and hydrophobic faces, and can be quantified in a helix structure as the polar angle [4,5]. Many studies of natural and synthetic peptides associate reduced polar angle with increased cell membrane permeabilization as a consequence of greater hydrophobic surface [6–8]. However, aggregation and the self-assembly process of AMPs have also been related to smaller polar angles [9,10]. The self-organization of peptide molecules can take place prior to or during membrane association, leading to highly stable supramolecular nanostructures, which are responsible for resistance to protease degradation in several cases [11].

Bacterial and fungal membranes have different phospholipid compositions as well as net charges. While the bacterial membrane is rich in anionic phosphatidylglycerol, the fungal and other eukaryotic

* Corresponding author at: LASEB, Departamento de Química, Universidade Federal dos Vales do Jequitinhonha e Mucuri, 39100-000 Diamantina, MG, Brazil.
E-mail address: verly.rodrigo@ufvjm.edu.br (R.M. Verly).

https://doi.org/10.1016/j.bbamem.2020.183449
Received 28 April 2020; Received in revised form 8 August 2020; Accepted 17 August 2020
Available online 21 August 2020

membranes are mainly composed of phospholipids with zwitterionic phosphatidylcholine headgroups [12]. Although the fungal membrane contains phospholipids with anionic phosphatidylinositol and phosphatidylserine headgroups, the large amount of zwitterionic phospholipids makes the membrane charge predominantly neutral [12]. The mode of action of AMPs is directly dependent on how they interact with these phospholipid membranes and several techniques, usually focused on structural and biophysical information, have been widely employed to investigate the peptide–membrane interaction [13]. Typically, the preferred systems for these studies are based on biomimetic environments, such as detergent micelles and phospholipid vesicles, where the charge is the main variable [14].

In this study, we investigate the mode of action of the 14-amino-acid-residue antimicrobial peptide HSP1-NH_2 (GILDAIKAIAK-AAG-NH_2), which is the C-terminal amidated derivative of hylaseptin P1 (HSP1), originally isolated from the skin extract of *Hyla punctata*, a frog found in the wetlands of the north and northeast regions of Brazil [15]. This peptide shows a moderate antibacterial activity against Gram-positive and Gram-negative strains, although its minimal inhibitory concentration (MIC) is similar to that of fluconazole [16] when tested against the pathogenic *Candida albicans* fungus [15]. To gain an insight into the apparent difference in the ability of HSP1-NH_2 to act as an antimicrobial against bacteria and fungi, we present a consistent set of results for the interactions of this peptide with anionic and zwitterionic model membranes. To comprehend different aspects of these interactions, we used several structural and biophysical approaches, including nuclear magnetic resonance (NMR) spectroscopy, circular dichroism (CD) spectroscopy, Fourier-transform infrared spectroscopy (FTIR), isothermal titration calorimetry (ITC), dynamic light scattering (DLS), zeta potential (ζP) and carboxyfluorescein leakage (CF).

2. Material and methods

2.1. Reagents

Peptide synthesis and purification: 4-Methylpiperidine (4-PIPE), triisopropylsilane (TIS), 1-hydroxybenzotriazole (HOBt), *N*,*N*′-diisopropylcarbodiimide (DIC), and also the amino acid derivatives (Fmoc-amino acids) were purchased from Sigma Aldrich (St Louis, USA); Isopropyl alcohol (IPA), trifluoroacetic acid (TFA) were purchased from Synth (Diadema, BRA); Dichloromethane (DCM) was purchased from Isofar (Duque de Caxias, BRA); *N*,*N*-Dimethylformamide (DMF) was acquired from Vetec Química Fina (Rio de Janeiro, Brazil). The resin, Rink amide, was purchased from NovaBiochem (Darmstadt, DEN). Acetonitrile (ACN) UV/HPLC grade was purchased from Panreac (Barcelona, SPA).

Preparation of phospholipid vesicles and detergent micelles: The lipids 1-palmitoyl-2-oleoyl-*sn*-glycero-3-phosphocholine (POPC) and 1-palmitoyl-2-oleoyl-*sn*-glycero-3-[phospho-*rac*-(1-glycerol)] (POPG) and the detergents dodecyl phosphocholine (DPC) and sodium dodecyl sulfate (SDS) were purchased from Avanti Polar Lipids (Alabaster, USA). The deuterated detergents dodecyl phosphocholine (DPC-d_{38}) and sodium dodecyl sulfate (SDS-d_{25}) were purchased from Cambridge Isotope Laboratories. The Sephadex G-25 medium, and 5(6)-carboxyfluorescein (CF) from Sigma-Aldrich (St Louis, USA). Milli-Q water was used in all studies.

2.2. Peptide synthesis

HSP1-NH_2 was manually synthesized by the solid phase method [17] on Rink-amide resin (substitution degree: 0.79 mmol.g^{-1}). Deprotection reactions were performed with 20% (*v*/v) 4-PIPE/DMF for 30 min (two 15 min steps) and coupling reactions with the respective amino acid derivative and DIC/HOBT in DMF during 120 min. After each deprotection and coupling steps, the resin was alternately washed three times with DMF, DCM and IPA, in this order. When the synthesis was completed, the peptide was cleaved from the resin by reacting the peptidyl-resin with 2 mL of a TFA:TIS:H_2O (95:2.5:2.5, v:v:v) solution for 60 min at room temperature. Cold diisopropyl ether was used to precipitate the peptide, which was extracted with water and lyophilized.

The crude peptide was purified by RP-HPLC in an analytical column (Vydac C18 250 × 4.6 mm) from Grace (Columbia, MD). The mobile phases were A – H_2O:ACN (100:0), 0.10% TFA and B – H_2O:ACN (0:100), 0.08% TFA. A gradient from 0 to 100% of B was used at a flow rate of 0.8 mL.min^{-1}. The purification was performed at room temperature and the chromatogram was recorded at 215 nm. The pure peptide was identified by MALDI-ToF mass spectrometry (Ultraflex III ToF-ToF – Bruker Daltonics, USA) in the reflected and positive mode, using α-cyano-4-hydroxycinnamic acid as matrix.

2.3. Preparation of Large Unilamellar Vesicles (LUV)

POPC and POPC:POPG (3:1, mol:mol) were co-solubilized in chloroform and then the organic solvent was removed in rotary evaporator at 40 °C to form a 50 μmol lipid film. Large multilamellar vesicles (LMV) were spontaneously formed when the dried film was suspended in the 10 mM Tris-HCl buffer (pH 8.5) by vigorous vortexing. Subsequently, LMV solution was freeze-thawing (8 cycles), alternating a liquid nitrogen and a water bath at 40 °C, followed by extrusion. The extrusion was performed at room temperature with a mini-extruder (Avanti Polar Lipids, Inc.) through 8 steps by using membranes of polycarbonate Nucleopore Track-Etch filters (Whatman-GE Healthcare) of 100 nm diameter. For each experiment, the LUV were prepared and used immediately.

For the preparation of the 5(6)-carboxyfluorescein (CF)-loaded vesicles, the 50 μmol lipid film was hydrated with 1.0 mL of a solution 10.0 mM Tris-HCl buffer pH 8.5 containing 50.0 mM CF. Free CF was removed by passing 1.0 mL of the extruded LUV in a Sephadex-G25 column (0.8 cm × 10 cm) eluted with 10 mM Tris–HCl, pH 8.5 containing 300 mmol.L^{-1} NaCl. The LUV were collected at the V_o and immediately used for assays.

2.4. Circular dichroism spectroscopy

The conformational preferences of HSP1-NH_2 were investigated in the presence of SDS and DPC micellar solutions, containing phosphate buffer (pH 7.6 and 5.8) as well as in the presence of unilamellar vesicles of POPC and POPC:POPG (3:1, mol:mol), containing 20 mM Tris-HCl buffer (pH 8.5). The spectra were recorded at 25 °C on a JASCO® J-810 spectropolarimeter (Tokyo, Japan), equipped with Peltier Jasco® temperature control system - PFD-425S (Tokyo, Japan), using a λ range from 190 to 260 nm. A quartz cuvette with 1 mm optical path was used and six scans were accumulated for samples containing DPC or SDS micelles and eight scans for samples containing POPC and POPC:POPG LUV. The samples were planned to contain 38 μM of HSP1-NH_2 at different concentrations of micellar detergents or phospholipids. Similar experiments were performed with blank solutions to allow for background subtraction. The data processing and estimation of secondary structure contents were carried out by using the CDPro and Spectra Analysis programs [18,19]. The estimations of helical content were obtained using the reference set of 48 proteins (basis set 7 of CDPro) in a wavelength range of 190–260 nm. Three methods (SELCON3, CDSSTR, and CONTIN/LL) were used for deconvolution and the average value of helicity was presented.

2.5. NMR spectroscopy

NMR spectra of 1.0 mM HSP1-NH_2 in the presence of both 200 mM DPC-d_{38} and SDS-d_{25} micelles were acquired at 25 °C on a Bruker Avance III 500 spectrometer (Rheinstetten, Germany). All the samples contained 0.5% of 3-trimethylsilyl-propionic-2,2,3,3-d_4 acid sodium

salt (TMSP) for internal reference and 10% D_2O for equipment lock.

$^1H-^1H$ TOCSY experiments were acquired with 4 k × 256 points (direct and indirect dimensions), 96 scans and mixing time of 80 ms. $^1H-^1H$ NOESY experiments were acquired with 4 k × 512 points, 114 scans and mixing time of 200 ms. Water signal suppression was achieved applying Watergate 3-9-19 [20,21]. $^1H-^{13}C$ HSQC spectra were recorded with 4 k × 150 points and 150 scans. $^1H-^{15}N$ SOFAST-HMQC experiments were acquired with 1 k × 100 points and 2048 scans. All the spectra were processed and analyzed using NMRPipe and NMRView, respectively [22,23]. The Wüthrich method [24] was used for the complete assignment of the ^1H resonances detected in TOCSY and NOESY spectra. The $^1H-^{15}N$ and $^1H-^{13}C$ heteronuclear spectra provided an extra control for the chemical-shift assignments.

The calculation of the three-dimensional structures was performed employing distance and dihedral angle restraints. The NOE correlations, classified as strong, medium and weak according to their volumes, were semi-quantitatively converted into distance upper limits of 2.8, 3.4 and 5.0 Å, respectively. Dihedral angle restraints were determined from the chemical shifts of $^1H\alpha$, $^1H\beta$, $^{13}C\alpha$ and $^{13}C\beta$ by using the TALOS+ program [25] of the NMRPIPE suite of software [22]. In order to obtain the three-dimensional structures, a simulated annealing protocol [26] of the program XPLOR-NIH was used [27]. 100 structures were generated and refined using the protocol "prot_sa_water_refine_nogyr.inp" [27,28]. Structures were visualized using the MOLMOL program [29]. The quality of the structures was analyzed based on the minimum values of root mean square deviation (RMSD) in the MOLMOL program and the Ramachandran diagram through the ICING online platform (https://nmr.cmbi.ru.Nl/icing/).

To monitor $^1H-^2H$ exchange [30], ^1H NMR spectra were recorded on a 500 MHz Bruker Avance III spectrometer using HSP1-NH_2 (1.0 mM) in presence of 200 mM of DPC-d_{38} micelles containing 5% of D_2O (v:v) or 50% of D_2O (v:v). The experiments were performed at 25 °C until 12 h after sample preparation.

2.6. Isothermal Titration Calorimetry (ITC)

The titration consisted of 15 successive injections of 10 μL of 190 μM HSP1-NH_2 into 20 mM POPC or POPC:POPG (3:1, mol:mol) LUV solutions in the presence of 10 mM Tris-HCl aqueous buffer (pH 8.5) at 303.15 K. Injection times of 2 s with intervals of 240 s have been used in the experiments. All solutions were previously degassed using simultaneously ultrasound bath and vacuum (140 mbar, 8 min) to eliminate air bubbles [31]. The Isothermal Titration Calorimetry (ITC) experiments were carried out on a Malvern® VP-ITC microcalorimeter (Malvern, UK) and the isotherms were processed and analyzed with the software Microcal Origin® 6.0 for ITC (Wellesley Hills, USA). The respective heat of dilution (h_c) was subtracted from the heat of reaction (h_i) for each titration. The binding enthalpies, ΔH, were calculated by dividing the corrected heat of reaction ($\delta h_i = h_i - h_c$) by the amount of injected peptide [32].

2.7. Dynamic light scattering and zeta potential (ζ)

The hydrodynamic diameter (D_h) and zeta potential (ζ) of 1.0 mM LUV were measured in a Malvern Zetasizer Nano ZS® particle analyzer (Malvern Instrument Ltd., Worcestershire, GRB) equipped with a 632.4 nm laser. The experiments were carried out titrating 500 μM POPC or POPC:POPG (3:1) LUV solutions with HSP1-NH_2, all diluted in 20 mM Tris-HCl buffer (pH 8.5), until a maximum peptide concentration of 0.2 mM. The experiments were performed at room temperature. The dynamic light scattering experiments were conducted in a 1.0 mL quartz cuvette (Malvern, Model DTS1060) and the zeta potential experiments were performed using a 700 μL folded capillary zeta cell (Malvern, DTS1061).

2.8. Carboxyfluorescein leakage

The carboxyfluorescein (CF) leakage experiments consisted in five independent continuous measurements of CF fluorescence at λ_{em} = 512 nm and λ_{ex} = 490 nm, released from (140 μM) POPC and (145 μM) POPC:POPG LUV after addition of HSP1-NH_2. The increase in fluorescence intensity was recorded as a function of time for each peptide concentration (ranging from 1.5 μM to 24 μM). After 3400 s, 10 μL of 10% Triton X-100 (*v*/v) solution were added to obtain complete vesicle leakage and the maximum CF fluorescence. The percentage of CF leakage was calculated according to eq. 1,

$$\%Leakage = \frac{I_0 - I_t}{I_0 - I_T} \times 100 \quad (1)$$

where I_o is the fluorescence before addition of HSP1-NH_2, I_t is the measured time-dependent fluorescence after peptide addition and I_T the fluorescence after Triton X-100 addition. All fluorescence measurements were performed in a SpectraMax (Molecular Devices, LCC) fluorimeter using a 1 mL quartz cuvette.

2.9. Surface plasmon resonance

The peptide–membrane interaction was also assessed by surface plasmon resonance measurements acquired on a Multi-Parametric Surface Plasmon Resonance BioNavis model SPR NAVI 200 (BioNavis®, Ylöjärvi, Finland) instrument. Stock solutions of POPC and POPC:POPG suspended in chloroform at 1.0 mM, were pipetted on the SiO_2 sensor chip (SPR102-SiO_2) surface and air dried. The analysis initially consisted of the passage of water over the sensor ship for laser calibration, followed by the exchange for 10 mM Tris-HCl buffer pH 8.0. The flow of buffer solution was kept constant (50 μL.min^{-1}). The equilibrium condition for all experiments was achieved by the running buffer (10 mM Tris-HCl buffer, pH 8.0) after approximately 20 min. The experiments consisted of injection of peptide (250 μL) at different concentrations in the phospholipid coating sensor chip. The ideal concentration for each system was evaluated by successive tests with the equipment. The systems which presented homogeneous signal were chosen to perform the analysis. All experiments were recorded at 670 nm. After each analysis, the sensorchip was washed in situ using sequential 5 min injections of 5% Hellmanex III®, isopropyl alcohol and milli-Q® water [16]. The kinetic parameters of the peptide-membrane interaction were obtained for the two biomimetic systems with TraceDrawer *v*.1.6 software (Ridgeview Instruments AB, Vänge, SWE).

2.10. FTIR spectroscopy

The FTIR measurements were carried out on a Varian 680 IR spectrometer equipped with a Gladi ATR optical design and a heat plate (Pike Technologies, Madison, USA). After 10 min of equilibration time at each temperature, the spectra were recorded from 30 to 50 °C at intervals of 2 °C as the average of 12 measurements, each with 32 scans with a spectral resolution of 4 cm^{-1}. All data were recoded and processed with the Resolutions Pro software. 20 mM DPPC or DPPG LUV solutions were suspended in 20 mM Tris-HCl buffer (pH 8.5) in the absence or in the presence of HSP1-NH_2 at 60 μM or 160 μM. The respective spectra of the Tris-HCl buffer (10 mM, pH 8.0) were recorded to allow background subtraction. The wavenumber for the symmetric CH_2 stretching ($\nu_s(CH_2)$) mode was determined by a multiple Gaussian curve fitting procedure (implemented in Origin 9) in the region between 3000 and 2750 cm^{-1}.

2.11. Accession numbers

NMR assignments and atomic coordinates of HSP1-NH_2 in presence of SDS-d_{25} and DPC-d_{38} micelles have been deposited in the Biological Magnetic Resonance Bank (30,744 and 30,745) and in the RCSB Protein

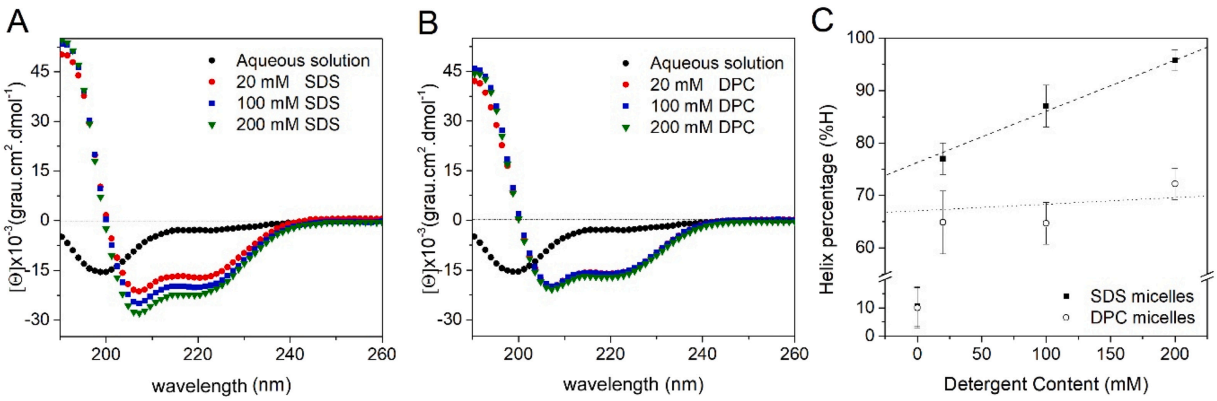

Fig. 1. CD spectra of HSP1-NH_2 in the absence or presence of (A) SDS and (B) DPC micelles. (C) Percentage of helical conformation (%H) as function of the detergent concentration. Trend lines (average between points, except for aqueous solution) in both systems are represented by dash and dots for SDS and DPC micelles, respectively. Helical contents were averaged from estimations by three different methods available in CDPro, namely SELCON, CDSSTR, and CONTIN/LL [18].

Data Bank (6WPB and 6WPD), respectively.

3. Results

3.1. Structural studies

The purified peptide was characterized by MALDI-ToF spectrometry (Fig. S1) and a single peak was observed at *m/z* 1310.79 ($M + H^+$), which is consistent with the molecular mass of the hylaseptin P1-NH_2 (theoretical $M + H^+$ m/z 1310.799). The conformational behavior of HSP1-NH_2 in the presence and absence of micellar buffer was assessed by circular dichroism spectroscopy. In aqueous solution a negative maximum at ~200 nm was observed, which indicates a disordered conformation (Fig. 1A, black circles). In the presence of either DPC or SDS micelles, even at low detergent concentrations (~ 20 mM), negative maxima characteristic of helical structures were observed at ~208 and 222 nm (Fig. 1A and B). Interestingly, in the presence of anionic micelles the HSP1-NH_2 helical content increased accordingly to the SDS concentration, whereas the helical content virtually did not change with the increase of the DPC concentration (Fig. 1B). This is clearly observed in the Fig. 1C, where the helix percentage (%H) increases linearly with the SDS concentration and virtually remains the same at different DPC concentrations [33].

The structural gain in the presence of either anionic or zwitterionic micelles evidence the interaction of the peptide with both systems. Therefore, we decided to investigate in the presence of both micelles the three-dimensional structures of HSP1-NH_2 at atomic level by solution NMR methodologies. The experiments were carried out in the presence of deuterium labeled SDS-d_{25} and DPC-d_{38} micelles. Two-dimensional $^1H-^1H$ TOCSY, $^1H-^1H$ NOESY and $^1H-^{13}C$ HSQC contour maps were acquired for 1.0 mM HSP1-NH_2 suspended in aqueous solutions of SDS-d_{25} or DPC-d_{38} at 200 mM containing 5% D_2O (v:v). Although CD spectroscopy indicated similar helical contents in both micellar solutions (Fig. 1A and B), distinct dispersions of the amide resonances (Fig. S2 and Fig. S3) as well as consistent Cα chemical shift differences (Fig. S4) are noticed when the respective pairs of HSP1-NH_2 NMR spectra are compared to each other [34]. The characteristic amino acid spin systems were identified in the TOCSY contour map (Fig. S2) and the unequivocal assignments were achieved by sequential and medium range interresidual correlations identified in the NOESY contour maps (Fig. S3). Interestingly, the correlations involving the amino hydrogens of G1 residue were observed at 9.65 ppm in the presence of DPC-d_{38} micelles, whereas no correlations involving these amino hydrogens were noticed in the presence of SDS-d_{25} micelles. Two points are important here: (i) amino hydrogens of peptide N-termini are usually very labile [35], suggesting the existence of suitable interactions, which trap these hydrogens to be observable in the NMR spectra; (ii) the occurrence only in the spectra of the peptide in the presence of DPC-d_{38} micelles indicates distinct structural arrangements of the HSP1-NH_2 N-terminus in each of the micellar solutions.

Sequential and medium range NOE correlations ranging from Ile-2 up to the C-terminal carboxamide were observed in the NOESY spectrum of HSP1-NH_2 in the presence of SDS-d_{25} micelles (Fig. 2A). Differently, a smaller range, extending mainly from Ala-5 to the C-

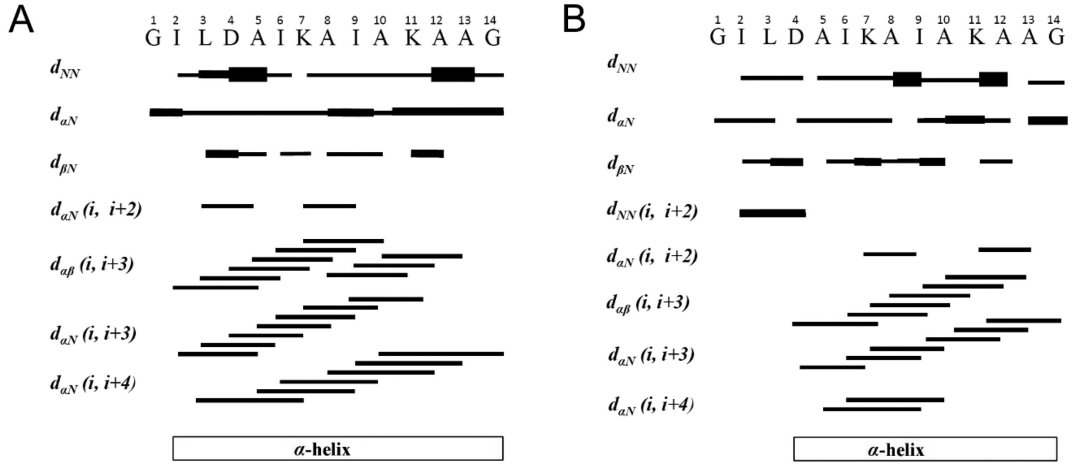

Fig. 2. Summary of the sequential and medium range NOE connectivities for HSP1-NH_2 in (A) SDS-d_{25} and (B) DPC-d_{38} micelles.

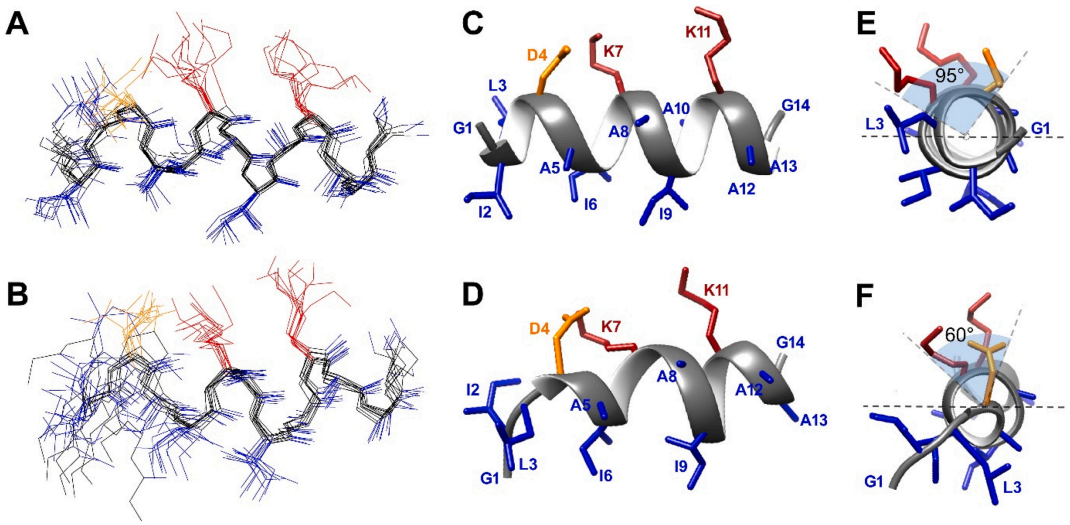

Fig. 3. Ribbon representation of HSP1-NH_2 lowest energy structures. Superposition of the 10 lowest energy structures of the peptide in the presence of (A) SDS-d_{25} and (B) DPC-d_{38} micelles. (B, C) Side and (E, F) frontal views of the structure closest to the average of the respective ensemble in the presence of (C, E) SDS-d_{25} and (D, F) DPC-d_{38} micelles, respectively. The positively charged hydrophilic side chains (lysines) are presented in red, the negatively charged side chain (aspartate) in orange and the hydrophobic side chains in blue. (E, F) The polar angles are represented by the shaded soft blue angles (95° in the presence of SDS-d_{25} micelles and 60° in the presence of DPC-d_{38} micelles). (For interpretation of the references to colour in this figure legend, the reader is referred to the web version of this article.)

terminus, was noted in the presence of DPC-d_{38} micelles (Fig. 2B).

The three-dimensional structures of HSP1-NH_2 in both media were calculated based on NOE distance and chemical shift dihedral angle restraints (Fig. 3). Both sets of structures showed significant amphipathic characters, where the positively charged Lys-7 and Lys-11 (highlighted in red) as well as the negatively charged Asp-4 (highlighted in orange) are located in the same face of the helix. Consequently, the hydrophobic face is virtually composed by uncharged and apolar residues. An interesting point is the considerably lower polar angle (60°) found for the peptide helix in the presence of zwitterionic micelles when compared to the helix polar angle in the presence of anionic micelles (95°) [6]. In addition, a slight bending of the helix is noticed near D4 in the presence of DPC-d_{38}, which drives the G1 and L3 residues towards the hydrophobic face (Fig. 3F). On the contrary, these residues are found in the interface of the hydrophilic and hydrophobic faces of the peptide helix in presence of SDS-d_{25} micelles (Fig. 3E).

The summary of the structural statistics of HSP1-NH_2 in presence of both SDS-d_{25} and DPC-d_{38} micelles is presented in Table S1. Considering only the well-structured α-helical segments in the ensemble of the 10 most stable structures, relatively small RMSD values are observed in both media, demonstrating a significant structural stability of these segments. When all residues are taken into account, slightly higher RMSD values are observed in both media, which is already expected due to the conformational dynamic observed near the amino-termini. The analyses of the Ramachandran plots (Fig. S5) indicate that 99.1% of the residues are found in the most favored regions of the diagram of HSP1-NH_2 in presence of SDS-d_{25}. On the other hand, the dihedral angles of Gly-1, Ile-2 and Ile-3 are located in the additional allowed regions (23.2%) in the presence of DPC-d_{38} micelles.

3.2. Thermodynamics of the interaction of HSP1-NH_2 with LUV

The enthalpic contribution of peptide–membrane interactions of HSP1-NH_2 with phospholipid vesicles were obtained in a quantitative manner from ITC experiments. In order to avoid the interference from heat of aggregation during membrane association, the experiments were carried out by titrating 10 μL of peptide solution (190 μM) into 1.48 mL of 10 mM POPC or POPC:POPG (3:1) LUV suspended in 10 mM Tris-HCl (pH 8.0) buffer (Fig. 4). The control experiment consisted in the peptide injection into buffer solution. The heat of peptide dilution is small (1.2 μcal/inj) and it is presented on the top of Fig. 4A and B. The raw data of the peptide–membrane binding indicate isothermal titration curves typical of exothermic-driven reactions with moderate affinity [36]. The value per injection derived from the integration of the titration peaks was approximately −28.5 μcal (Fig. 4A) in presence of anionic LUV and − 16.5 μcal in presence of zwitterionic LUV (Fig. 4B).

The heats of binding for each injection of HSP1-NH_2 to POPC and POPC:POPG (3:1) LUV are presented in the Fig. 4C and D, respectively. The molar enthalpies of binding (ΔH^o) were calculated from the cumulative heat of binding after each injection divided by the total amount of injected peptide. The enthalpic contribution of HSP1-NH_2 interacting with POPC:POPG LUV ($\Delta H^o = -2.2$ kcal.mol^{-1}) was about two times higher than the value obtained for the binding to POPC LUV ($\Delta H^o = -1.0$ kcal.mol^{-1}).

3.3. Effect of peptide-membrane interactions on phospholipid vesicles

The effects of the peptide–membrane interactions on the hydrodynamic diameters (D_h) and zeta potentials (ζP) of POPC and POPC:POPG (3:1) LUV were evaluated by dynamic light scattering (DLS) measurements (Fig. 5). All plotted data presented polydispersity index lower than 0.3, which is indicative of monodisperse vesicular population [37]. The size of both zwitterionic and anionic vesicles underwent similar increases (maximum $\Delta D_h \approx 20$ nm in POPC:POPG and $\Delta D_h \approx 22$ nm in POPC LUV) with the addition of peptide, as resulted from peptide–membrane adsorption [38]. Nevertheless, the effects of the addition of HSP1-NH_2 to each LUV solution were different in terms of peptide concentration. Whereas the diameter of POPC:POPG LUV increased proportionately with peptide concentration until 0.20 peptide-to-phospholipid ratio, an abrupt increment in the D_h was observed at the peptide-to-phospholipid molar ratio of 0.07 for POPC LUV (Fig. 5A).

The effects of HSP1-NH_2 addition on the zeta potential (ζP) of the two LUV solutions were rather different. The addition of peptide led to a continuous increases of the ζP of the anionic vesicles until a peptide-to-phospholipid molar ratio of 0.06, from which a plateau is reached (ζP ≈ − 20 mV). On the other hand, only small changes (ζP ≈ − 5 mV) are observed for POPC LUV even at high HSP1-NH_2 concentrations (Fig. 5B).

The lytic activity of HSP1-NH_2 on anionic and zwitterionic LUV was

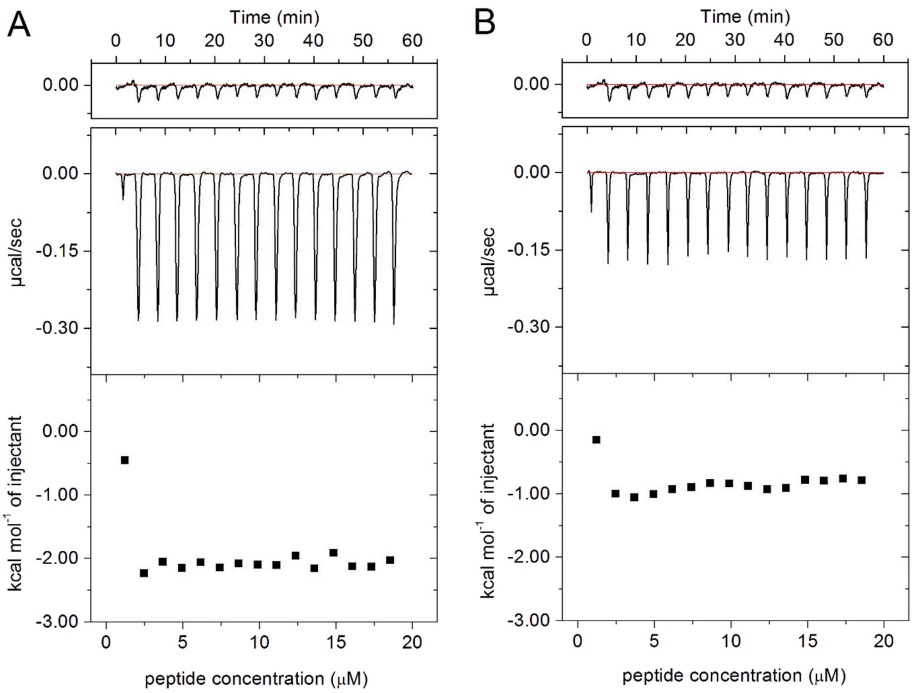

Fig. 4. Isothermal titration calorimetry of (A) 10 mM POPC:POPG (3:1) and (B) POPC with 190 µM HSP1-NH_2 (10 mM Tris, pH 8.0) at 30 °C. Aliquots (10 µL) of the peptide solution were added to the phospholipid suspension in the reaction cell. The reference cell contained the respective buffer solution (10 mM Tris, pH 8.5). The heats of peptide dilution are shown at the top. The panels at the middle show the calorimeter raw data. The respective heat flow per injection evaluated from the areas underneath the baseline is shown in the panels at the bottom.

assessed through carboxyfluorescein (CF) leakage experiments. The fluorescence intensity of CF released from POPC and POPC:POPG (3:1) vesicles was measured after peptide injection at different concentrations (Fig. 6). Clearly, in both media the peptide is able to disturb the membrane structure leading to CF releases of about 60% from POPC:-POPG LUV and 55% from POPC LUV. Again, the relationship between the peptide concentration and the disruptive effect on the bilayer differs markedly for the two membrane models. Increments in the HSP1-NH_2-to-phospholipid ratio lead to a proportional increase in the percentage of CF leakage of POPC:POPG LUV, achieving a plateau at about 0.08 M ratio. On the other hand, for assays with CF loaded POPC LUV, at small peptide-to-phospholipid molar ratios (> 0.05) no significant variations are observed in the percentages of dye release (e.g., about 20% at ~0.05 M ratio). Surprisingly, at HSP1-NH_2-to-phospholipid molar ratios of about 0.08 the percentage of CF released from POPC LUV reaches the maximum value of ~55%.

3.4. Surface plasmon resonance

A sensor chip covered with SiO_2 to phospholipid monolayer adsorption was used for the SPR experiments [39]. The POPC and POPC:POPG (3:1) stock solutions (1.0 mM) were applied on the sensor chip surface and HSP1-NH_2 solutions at six different concentrations were used in the measurements. Fig. 7 presents the superposition of the obtained sensorgrams. For both vesicles, the RU signal intensity increases as a function of the peptide concentration, which evidence the peptide–membrane affinity. Whereas the SPR signal increases in a stepwise manner for the POPC:POPG coating sensor chip, markedly higher response levels are observed only above 20 µM of HSP1-NH_2 for the POPC coating sensor chip. Fig. 7C shows the graphical sensorgram response levels as a function of the peptide-to-phospholipid molar ratio. The association constant K_a for each peptide–membrane system was calculated from the binding sensorgrams (affinity adjustment - *Affinity 50 in TraceDrawer* software) considering the model of one site binding. Although the binding sensorgrams presented remarkable distinct behaviors, the association constant of HSP1-NH_2 showed comparable values in the presence of POPC membrane (K_a = 8100 M^{-1}) when compared to the POPC:POPG membrane (K_a = 4900 M^{-1}).

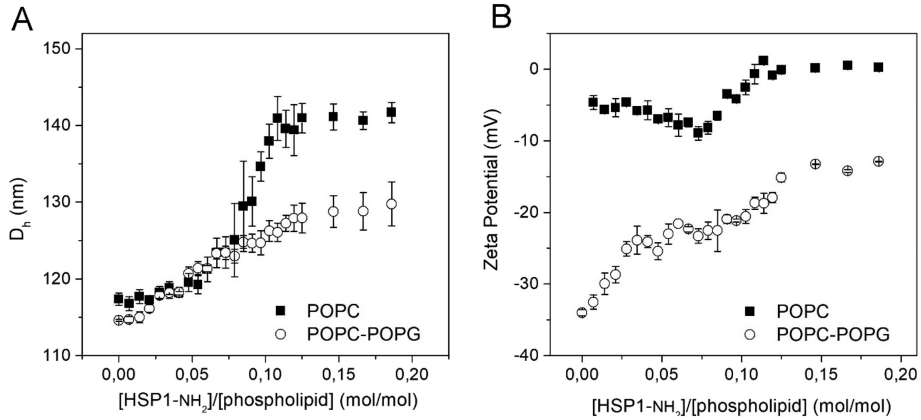

Fig. 5. (A) Hydrodynamic Diameter and (B) Zeta potential of POPC and POPC:POPG (3:1) LUV as a function of HSP1-NH_2/phospholipid molar ratio. The phospholipid vesicles at 1.0 mM were suspended in 10 mM Tris-HCl buffer at pH 8.5, 25 °C.

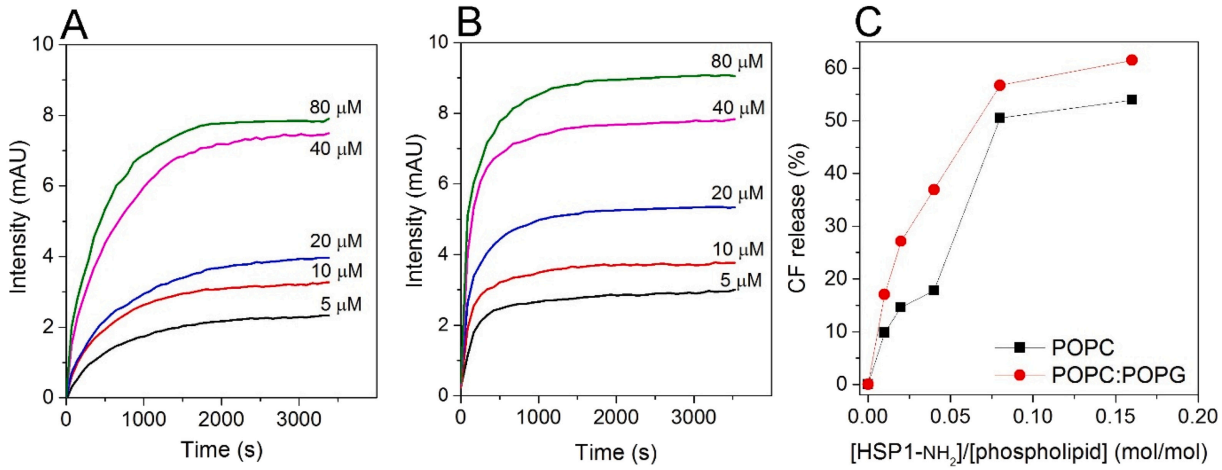

Fig. 6. Kinetics of carboxyfluorescein release from (A) 140 μM POPC and (B) 145 μM POPC:POPG LUV at 25 °C induced by HSP1-NH_2 at different concentrations. (C) The percentage of CF release at different peptide-to-lipid molar ratios were compared to the release measured after the addition of the control (10% Triton X-100) at 3400 s. The experiments were performed at 10 mM Tris-HCl pH 8.5 aqueous buffer containing 300 mM NaCl.

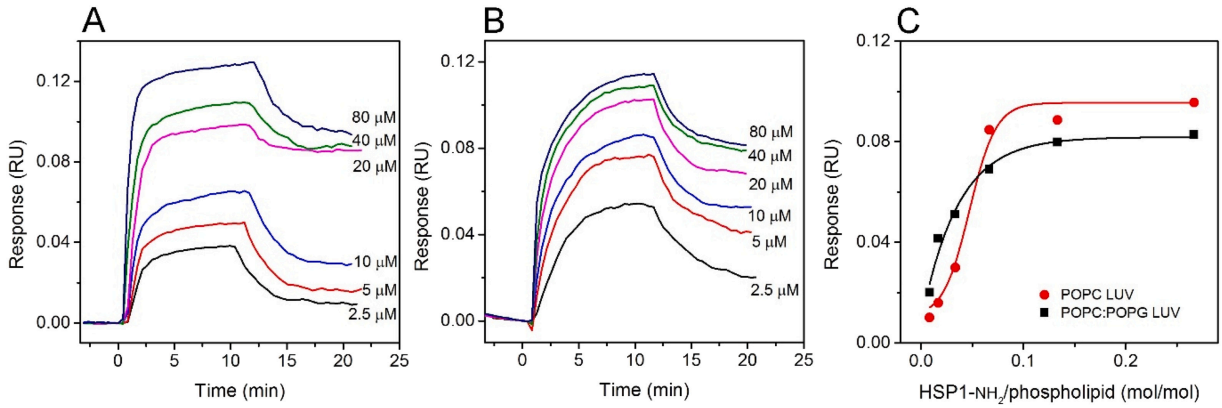

Fig. 7. SPR sensorgrams for the peptide–membrane interaction of HSP1-NH_2 with (A) POPC and (B) POPC:POPG (3:1) membranes. Phospholipids at 0.1 mM (10 mM Tris-HCl buffer, pH 8.0) were immobilized onto the surface of a SiO_2 sensor chip and the peptide was injected at 2.5, 5, 10, 20, 40 and 80 μM concentrations (10 mM Tris-HCl buffer, pH 8.0). (C) Non-linear fitting of the RU intensities as a function of the peptide-phospholipid molar ratio for POPC (red circles) and POPC:POPG (black squares) membranes. (For interpretation of the references to colour in this figure legend, the reader is referred to the web version of this article.)

3.5. FTIR spectroscopy

The effects of peptide binding on DPPC and DPPG lipid vesicles were examined by FT-IR spectroscopy in terms of the phospholipid acyl chain organization. The frequencies of the asymmetric $\nu_{as}(CH_2)$ and symmetric $\nu_s(CH_2)$ stretching bands were monitored at different temperatures employing low (0.03) and high (0.08) peptide-to-phospholipid molar ratios. Fig. S7 shows the region characteristic of $\nu_{as}(CH_2)$ and $\nu_s(CH_2)$ vibrational bands of the FT-IR spectra obtained for the HSP1-NH_2/DPPG 0.08 M ratio at one temperature below (32 °C) and another above (46 °C) the phase transition temperature. The gel phase ($L_{\beta'}$) is characterized by highly ordered acyl chains at *trans* conformation. In the liquid crystalline phase (L_α) the order is disturbed due to the increase of gauche fractions and the consequent decrease of van der Waals attractions [40]. Therefore, the $L_{\beta'} \rightarrow L_\alpha$ phase transition can be monitored by shifts from values ≤ 2850 cm^{-1} to 2852–2853 cm^{-1} [10,41,42].

Fig. 8A and B shows the temperature-dependence of the $\nu_s(CH_2)$ maximum absorption wavenumber for DPPC and DPPG membranes in the presence of the HSP1-NH_2. For DPPG vesicles, the addition of HSP1-NH_2 leads to shifts in wavenumber to lower values for all investigated temperatures at both peptide-to-phospholipid molar ratios. In turn, no significant changes are observed for DPPC membranes containing the peptide at the 0.03 M ratio, whereas at the 0.08 M ratio, a consistent shift of the vibrational mode wavenumbers to higher values is noticed at all investigated temperatures (Table 1). The phase transition temperature (T_m) for all systems was determined by the first derivative of the temperature-dependent curves (Fig. 8C and D). The addition of peptide leads to slight increases of the T_m for DPPG vesicles at both molar ratios, which is typically attributed to an increased ordering of the lipid acyl chains [40,43]. On the other hand, no significant change is observed for DPPC vesicles containing the peptide at 0.03 M ratio, while a consistent T_m increase is verified at the 0.08 M ratio (Table 1), suggesting some disordering of the acyl chains. Hence, HSP1-NH_2 only shows significant influence on the hydrophobic core of the DPPC membranes at higher peptide-to-phospholipid molar ratio [10].

4. Discussion

Wild-type HSP1 shows moderate antibacterial and antifungal potentials. Therefore, we decided to synthesize its C-terminal amidated analogue HSP1-NH_2, since carboxamidation is known to enhance the activity of several antimicrobial sequences [44]. This peptide has a high proportion of hydrophobic and neutral (78%) residues and, consequently, low cationic net charge (+2). Our study presents structural and biophysical experiments that correlate conformational features and aspects of the peptide–membrane interactions, which indicate divergent modes of association of HSP1-NH_2 to anionic and zwitterionic

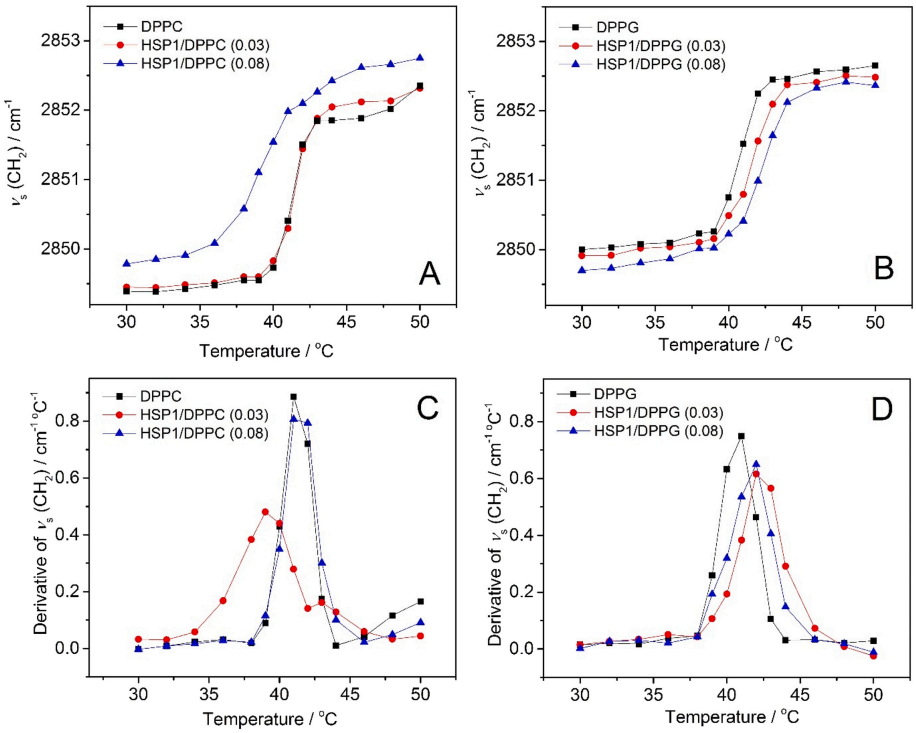

Fig. 8. (A, B) $\nu_s(CH_2)$ maximum absorption wavenumber as a function of temperature for (A) DPPC and (B) DPPG in the absence or in the presence of HSP1-NH_2 at different peptide-to-phospholipid molar ratios. The respective first derivatives for (C) DPPC and (D) DPPG membranes.

Table 1
Shifts of the maximum absorption wavenumbers of $\nu_s(CH_2)$ observed by FT-IR for peptide/DPPC and peptide/DPPG mixtures (0.03 and 0.08 M ratio) with respect to pure DPPC and DPPG membranes, respectively, in the gel state ($\Delta\nu_s(CH_2)$32 °C) or fluid state ($\Delta\nu_s(CH_2)$46 °C) (100 mM NaCl in D_2O).

Sample	$\Delta\nu_s(CH_2)_{32°C}/cm^{-1}$	$\Delta\nu_s(CH_2)_{46°C}/cm^{-1}$	ΔT_m/°C
DPPC			
HSP1/DPPC (0.03)	−0.06	−0.23	−0.20
HSP1/DPPC (0.08)	−0.47	−0.63	−2.50
DPPG			
HSP1/DPPG (0.03)	0.11	0.15	0.80
HSP1/DPPG (0.08)	0.30	0.23	1.50

membranes.

Conformational analyses showed that the HSP1-NH_2 acquires a higher helical content in the presence of SDS micelles than in the presence of DPC micelles (Fig. 1). Interestingly, micellar concentration–dependence of the helical content was evident only in the anionic medium (Fig. 1C), suggesting distinct binding processes in the two media. In this way, the conformational differences at atomic level were assessed by solution NMR experiments (Fig. 3). A canonical helical conformation extending from I2 to the peptide C-terminus was noted in the presence of SDS-d_{25} micelles (Fig. 3A, C), with a higher convergence of the backbone and side chains atoms (RMSD = 0.64 ± 0.15 Å). As expected, the extent of helical conformation (from A5 to C-terminal) was less in the presence of DPC-d_{38} micelles (Fig. 3B, D), and the structure of the polypeptide chain was less ordered (RMSD = 0.92 ± 0.28 Å).

In DPC-d_{38} micelles, helix bending was observed near D4 (Fig. 3D, F), which drove G1 and L3 to the hydrophobic face of the helix. Distortions at the helix N-terminus may be associated with helix folding as a result of partial insertion of polypeptide chain [45,46]. Interestingly, the quite unusual observation of the amino N-terminal hydrogen resonances indicates its partial insertion into the micelle interface, making it detectable by solution NMR spectroscopy. Several reports have described the insertion of glycine N-terminus as a determinant of the orientation and interaction of influenza haemagglutinin fusion peptides [47–49]. The insertion of the peptide N-terminus into the DPC-d_{38} micelles was evaluated by ^2H exchange NMR experiments (Fig. S6). Following increase of the D_2O concentration in the sample, the amino hydrogen resonance signal of G1 retained its relative intensity in the NMR spectrum even 12 h after sample preparation. Similarly, intense signals were also observed for the amide hydrogens of I2 and L3, which provides even more evidence of the N-terminus insertion into the micelle interface. In addition, the low-field chemical shift of G1 HN (9.65 ppm) is indicative of the stabilization of the charged amino group by electrostatic interactions with the phosphate headgroups [50]. On the other hand, these structural features of the HSP1-NH_2 N-terminus are not observed in the presence of anionic micelles and consequently the structural arrangement of the peptide N-terminus varies considerably between these micellar environments. In addition, the higher conformational flexibility of N-terminal portion in the presence of the DPC-d_{38} micelles suggest different modes of action for HSP-1 in both media [51]. Therefore, the high-resolution NMR structures demonstrate in atomic details the existence of distinct aspects regarding the membrane interactions of HSP1-NH_2, which are strongly dependent on membrane composition.

Investigations of the thermodynamics of peptide-membrane interactions showed a higher enthalpic factor for the association of HSP1-NH_2 with anionic LUV when compared to zwitterionic LUV, suggesting better establishment of electrostatic interactions of the peptide in POPC:POPG vesicles. This finding is in line with the NMR structures (Fig. 3A), since a more linear amphipathic helical conformation optimizes the in-plane contacts of the peptide with the bilayer surface [52]. In the presence of anionic vesicles (POPC:POPG, 3:1), the peptide–membrane interaction seemed to be linearly dependent on the peptide concentration. The effect of HSP1-NH_2 in both D_h changes (Fig. 5) and dye release (Fig. 6) from CF-loaded anionic LUV increased proportionately to the peptide-to-phospholipid ratio until reaching a plateau. Similarly, SPR data showed continuous increases in sensorgram level responses, with the maximum value near to a peptide-to-phospholipid

molar ratio of 0.08. Interestingly, slight decreases in both $\nu_s(CH_2)$ stretching wavenumbers and the melting phase transition (T_m) of DPPG LUV were observed at the both investigated peptide-to-phospholipid molar ratios (Table 1). These results are in accordance with the predominance of electrostatic interactions that lead to peptide orientations approximately parallel to the membrane surface. Accordingly, peptide binding to the lipid headgroups can limit lipid motion, which reduces the rotational freedom of the acyl chains and at the same time decreases the $\nu_s(CH_2)$ wavenumber and T_m [53]. All of these results, allied to the greater changes in the zeta potential up to the HSP1-NH_2-to-POPC:-POPG molar ratio of 0.06, suggest that the interactions of HSP1-NH_2 with anionic biomembranes occur according to a carpet-like mechanism, similar to the mode of action suggested by Chen et al. (2020) for the wild-type HSP1 peptide [54].

On the other hand, the smaller enthalpic contribution in the presence of zwitterionic LUV suggests the prevalence of hydrophobic effects [55,56] and a distinct mechanism of interaction between HSP1-NH_2 and the zwitterionic membrane. Self-assembling peptides also show reduced enthalpic contributions due to the high content of hydrophobic residues. This imposes conditions where the establishment of electrostatic interaction is not favorable (less favorable ΔH^0), which leads to aggregation even in the membrane environment [57]. Self-aggregation process of peptides cause a sudden increase in the phospholipid vesicle size during the interaction [14], as observed for POPC LUV (Fig. 5A) after injection of HSP1-NH_2 at high peptide-to-phospholipid molar ratios (> 0.07). Thus, HSP1-NH_2 appears to interact effectively with zwitterionic vesicles only after reaching a minimum critical concentration on the LUV surface, as also noted in the CF release, SPR, and FITR experiments.

Although some degree of carboxyfluorescein leakage could be observed even at lower HSP1-NH_2-to-POPC molar ratios (0.01 to 0.04), meaning that some initial structural perturbation occurred independently of changes in vesicle diameter, substantial lytic activities were noticed only at molar ratios greater than 0.06. Similar behavior was evident in the SPR measurements (Fig. 7A), in which minor changes were observed in the sensorgrams at low peptide concentrations (≤ 20 mM), whereas at high peptide-to-phospholipid molar ratios (peptide concentration $>$ 20 mM) abrupt response levels were verified in the assays with zwitterionic membranes. In addition, both $\nu_s(CH_2)$ stretching wavenumbers and the melting phase transition temperatures (T_m) of DPPC membranes underwent noticeable increases (Table 1) only upon premixing with HSP1-NH_2 at the highest peptide-to-phospholipid molar ratio (0.08) investigated. Taken together, these results indicate the disruption of the bilayer arrangement as a consequence of the close contact between HSP1-NH_2 and the hydrophobic inner part of the membrane [10]. The small change in zeta potential ($\Delta\zeta P \approx 5$ nm) also indicates the prevalence of hydrophobic interactions of HSP1-NH_2 with zwitterionic vesicles (POPC; Fig. 5B). This behavior confirms a non-superficial interaction, which suggests the insertion of the peptide on the membrane interface due to a hydrophobic effect [58] that is dependent on the peptide concentration and on the structure of the peptides within the aggregate. This is corroborated by the smaller polar angle of the helix in the presence of zwitterionic micelles (Fig. 3F), which is correlated in some cases to the aggregation and self-assembly process [59].

Given the predominantly neutral charge of fungal membranes and the predominantly negative charge of bacterial membranes, the distinct binding processes of the peptide to zwitterionic and anionic biomembranes seem to be partly related to the higher activity against *C. albicans* than against *S. aureus*.

5. Conclusions

Several techniques have been used to investigate the interactions of the antimicrobial peptide HSP1-NH_2 with zwitterionic and anionic membranes. Complementary information was obtained from the different approaches, which gave several insights into peptide–membrane binding as well as into membrane disruption processes. Important differences were noted in the mechanisms of interaction of HSP1-NH_2 with POPC and POPC:POPG membranes. Interactions with anionic membranes showed a gradual dependence on the peptide concentration, whereas interactions with zwitterionic membranes were rather more superficial until a critical peptide-to-phospholipid ratio around 0.06 was reached, at which peptide membrane insertion and disruption took place effectively.

Declaration of competing interest

The authors declare that they have no known competing financial interests or personal relationships that could have appeared to influence the work reported in this paper.

Acknowledgements

IPG, ANS, COM and GAC acknowledge grants from Coordenação de Aperfeiçoamento de Pessoal de Nível Superior (CAPES). TLS acknowledges a grant from PNPD/CAPES. JMR and LML acknowledge grants from Conselho Nacional de Desenvolvimento Científico e Tecnológico (CNPq). This work is a collaboration research project of members of the Rede Mineira de Química (RQ-MG). We also appreciate the contribution from the funding agencies CNPq, Fundação de Amparo à Pesquisa do Estado de Minas Gerais (FAPEMIG), CAPES and PRPPG-UFVJM.

Appendix A. Supplementary data

Supplementary data to this article can be found online at https://doi.org/10.1016/j.bbamem.2020.183449.

References

[1] P.Y. Chung, R. Khanum, Antimicrobial peptides as potential anti-biofilm agents against multidrugresistant bacteria, Journal of Microbiology Immunology and Infection 50 (2017) 405–410.
[2] D. Ciumac, H.N. Gong, X.Z. Hu, J.R. Lu, Membrane targeting cationic antimicrobial peptides, J. Colloid Interface Sci. 537 (2019) 163–185.
[3] L.T. Nguyen, E.F. Haney, H.J. Vogel, The expanding scope of antimicrobial peptide structures and their modes of action, Trends Biotechnol. 29 (2011) 464–472.
[4] M.R. Yeaman, N.Y. Yount, Mechanisms of antimicrobial peptide action and resistance, Pharmacol. Rev. 55 (2003) 27–55.
[5] D. Ciumac, H. Gong, X. Hu, J.R. Lu, Membrane targeting cationic antimicrobial peptides, J. Colloid Interface Sci. 537 (2019) 163–185.
[6] N. Uematsu, K. Matsuzaki, Polar angle as a determinant of amphipathic α-helix-lipid interactions: a model peptide study, Biophys. J. 79 (2000) 2075–2083.
[7] T. Wieprecht, M. Dathe, R.M. Epand, M. Beyermann, E. Krause, W.L. Maloy, D.L. MacDonald, M. Bienert, Influence of the angle subtended by the positively charged helix face on the membrane activity of amphipathic, antibacterial peptides, Biochemistry 36 (1997) 12869–12880.
[8] S.-K. Zhang, J.-w. Song, F. Gong, S.-B. Li, H.-Y. Chang, H.-M. Xie, H.-W. Gao, Y.-X. Tan, S.-P. Ji, Design of an α-helical antimicrobial peptide with improved cell-selective and potent anti-biofilm activity, Sci. Rep. 6 (2016) 1–13.
[9] A. Zemel, D.R. Fattal, A. Ben-Shaul, Energetics and self-assembly of amphipathic peptide pores in lipid membranes, Biophys. J. 84 (2003) 2242–2255.
[10] E. Sikorska, M. Dawgul, K. Greber, E. Ilowska, A. Pogorzelska, W. Kamysz, Self-assembly and interactions of short antimicrobial cationic lipopeptides with membrane lipids: ITC, FTIR and molecular dynamics studies, Biochimica Et Biophysica Acta-Biomembranes 1838 (2014) 2625–2634.
[11] Z. Ye, X. Zhu, S. Acosta, D. Kumar, T. Sang, C. Aparicio, Self-assembly dynamics and antimicrobial activity of all l- and d-amino acid enantiomers of a designer peptide, Nanoscale 11 (2019) 266–275.
[12] D.E. Warschawski, A.A. Arnold, M. Beaugrand, A. Gravel, E. Chartrand, I. Marcotte, Choosing membrane mimetics for NMR structural studies of transmembrane proteins, Biochimica Et Biophysica Acta-Biomembranes 1808 (2011) 1957–1974.
[13] S. Galdiero, A. Falanga, M. Cantisani, M. Vitiello, G. Morelli, M. Galdiero, Peptide-lipid interactions: experiments and applications, Int. J. Mol. Sci. 14 (2013) 18758–18789.
[14] X.B. Tian, F.D. Sun, X.R. Zhou, S.Z. Luo, L. Chen, Role of peptide self-assembly in antimicrobial peptides, J. Pept. Sci. 21 (2015) 530–539.
[15] M.V. Prates, M.L. Sforca, W.C.B. Regis, J. Leite, L.P. Silva, T.A. Pertinhez, A.L.T. Araujo, R.B. Azevedo, A. Spisni, C. Bloch, The NMR-derived solution structure of a new cationic antimicrobial peptide from the skin secretion of the anuran Hyla punctata, J. Biol. Chem. 279 (2004) 13018–13026.

[16] E.F.C. Junior, C. Guimaraes, L.L. Franco, R.J. Alves, K.C. Kato, H.R. Martins, J.D. de Souza, M.P. Bemquerer, V.H.O. Munhoz, J.M. Resende, R.M. Verly, Glycotriazole-peptides derived from the peptide HSP1: synergistic effect of triazole and saccharide rings on the antifungal activity, Amino Acids 49 (2017) 1389–1400.
[17] R.B. Merrifield, Solid phase peptide synthesis. I. the synthesis of a tetrapeptide, J. Am. Chem. Soc. 85 (1963) 2149.
[18] N. Sreerama, R.W. Woody, Estimation of protein secondary structure from circular dichroism spectra: comparison of CONTIN, SELCON, and CDSSTR methods with an expanded reference set, Anal. Biochem. 287 (2000) 252–260.
[19] N. Sreerama, R.W. Woody, On the analysis of membrane protein circular dichroism spectra, Protein Sci. 13 (2004) 100–112.
[20] A. Bax, D.G. Davis, MLEV-17-based two-dimensional homonuclear magnetization transfer spectroscopy, J. Magn. Reson. 65 (1985) 355–360.
[21] M. Piotto, V. Saudek, V. Sklenar, Gradient-tailored excitation for single-quantum NMR spectroscopy of aqueous solutions, J. Biomol. NMR 2 (1992) 661–665.
[22] F. Delaglio, S. Grzesiek, G.W. Vuister, G. Zhu, J. Pfeifer, A. Bax, NMRPipe: a multidimensional spectral processing system based on UNIX pipes, J. Biomol. NMR 6 (1995) 277–293.
[23] B.A. Johnson, R.A. Blevins, NMR view: a computer program for the visualization and analysis of NMR data, J. Biomol. NMR 4 (1994) 603–614.
[24] K. Wuthrich, Protein structure determination in solution by NMR spectroscopy, J. Biol. Chem. 265 (1990) 22059–22062.
[25] Y. Shen, F. Delaglio, G. Cornilescu, A. Bax, TALOS plus: a hybrid method for predicting protein backbone torsion angles from NMR chemical shifts, J. Biomol. NMR 44 (2009) 213–223.
[26] L.M. Rice, A.T. Brunger, Torsion angle dynamics: reduced variable conformational sampling enhances crystallographic structure refinement, Proteins-Structure Function and Genetics 19 (1994) 277–290.
[27] C.D. Schwieters, J.J. Kuszewski, G.M. Clore, Using Xplor-NIH for NMR molecular structure determination, Prog. Nucl. Magn. Reson. Spectrosc. 48 (2006) 47–62.
[28] C.D. Schwieters, J.J. Kuszewski, N. Tjandra, G.M. Clore, The Xplor-NIH NMR molecular structure determination package, J. Magn. Reson. 160 (2003) 65–73.
[29] R. Koradi, M. Billeter, K. Wuthrich, MOLMOL: a program for display and analysis of macromolecular structures, J. Mol. Graph. 14 (1996) 51.
[30] K.A. Gomes, D.M. Dos Santos, V.M. Santos, D. Piló-Veloso, H.M. Mundim, L.V. Rodrigues, L.M. Lião, R.M. Verly, M.E. de Lima, J.M. Resende, NMR structures in different membrane environments of three ocellatin peptides isolated from Leptodactylus labyrinthicus, Peptides 103 (2018) 72–83.
[31] M. Rekharsky, Y. Inoue, S. Tobey, A. Metzger, E. Anslyn, Ion-pairing molecular recognition in water: aggregation at low concentrations that is entropy-driven, J. Am. Chem. Soc. 124 (2002) 14959–14967.
[32] T. Wieprecht, M. Beyermann, J. Seelig, Binding of antibacterial magainin peptides to electrically neutral membranes: thermodynamics and structure, Biochemistry 38 (1999) 10377–10387.
[33] Y.H. Chen, J.T. Yang, K.H. Chau, Determination of the helix and beta form of proteins in aqueous solution by circular dichroism, Biochemistry 13 (1974) 3350–3359.
[34] L.W. Tinoco, A. da Silva, A. Leite, A.P. Valente, F.C.L. Almeida, NMR structure of PW2 bound to SDS micelles - a tryptophan-rich anticoccidial peptide selected from phage display libraries, J. Biol. Chem. 277 (2002) 36351–36356.
[35] K. Wüthrich, NMR with proteins and nucleic acids, Europhysics News 17 (1986) 11–13.
[36] R.M. Verly, J.M. Resende, E.F.C. Junior, M.T.Q. de Magalhaes, C. Guimaraes, V.H.O. Munhoz, M.P. Bemquerer, F.C.L. Almeida, M.M. Santoro, D. Pilo-Veloso, B. Bechinger, Structure and membrane interactions of the homodimeric antibiotic peptide homotarsinin, Sci. Rep. 7 (2017).
[37] M. Danaei, M. Dehghankhold, S. Ataei, F. Hasanzadeh Davarani, R. Javanmard, A. Dokhani, S. Khorasani, M. Mozafari, Impact of particle size and polydispersity index on the clinical applications of lipidic nanocarrier systems, Pharmaceutics 10 (2018) 57.
[38] R.M. Verly, M.A. Rodrigues, K.R.P. Daghastanli, A.M.L. Denadai, I.M. Cuccovia, C. Bloch Jr., F. Frézard, M.M. Santoro, D. Piló-Veloso, M.P. Bemquerer, Effect of cholesterol on the interaction of the amphibian antimicrobial peptide DD K with liposomes, Peptides 29 (2008) 15–24.
[39] K. Hall, H. Mozsolits, M.I. Aguilar, Surface plasmon resonance analysis of antimicrobial peptide-membrane interactions: affinity & mechanism of action, Lett. Pept. Sci. 10 (2003) 475–485.
[40] L.K. Tamm, S.A. Tatulian, Infrared spectroscopy of proteins and peptides in lipid bilayers, Q. Rev. Biophys. 30 (1997) 365–429.
[41] M. Hoernke, C. Schwieger, A. Kerth, A. Blume, Binding of cationic pentapeptides with modified side chain lengths to negatively charged lipid membranes: complex interplay of electrostatic and hydrophobic interactions, Biochimica Et Biophysica Acta-Biomembranes 1818 (2012) 1663–1672.
[42] C. Schwieger, A. Blume, Interaction of poly(L-lysines) with negatively charged membranes: an FT-IR and DSC study, Eur. Biophys. J. Biophys. Lett. 36 (2007) 437–450.
[43] D.G. Cameron, H.L. Casal, H.H. Mantsch, Y. Boulanger, I.C.P. Smith, The thermotropic behavior of dipalmitoyl phosphatidylcholine bilayers. A Fourier transform infrared study of specifically labeled lipids, Biophys. J. 35 (1981) 1–16.
[44] M.L. Sforça, S. Oyama, F. Canduri, C.C. Lorenzi, T.A. Pertinhez, K. Konno, B.M. Souza, M.S. Palma, J. Ruggiero Neto, W.F. Azevedo, How C-terminal carboxyamidation alters the biological activity of peptides from the venom of the eumenine solitary wasp, Biochemistry 43 (2004) 5608–5617.
[45] D.M. Santos, R.M. Verly, D. Pilo-Veloso, M. de Maria, M.A.R. de Carvalho, P.S. Cisalpino, B.M. Soares, C.G. Diniz, L.M. Farias, D.F.F. Moreira, F. Frezard, M.P. Bemquerer, A.M.C. Pimenta, M.E. de Lima, LyeTx I, a potent antimicrobial peptide from the venom of the spider Lycosa erythrognatha, Amino Acids 39 (2010) 135–144.
[46] R.M. Verly, C.M. de Moraes, J.M. Resende, C. Aisenbrey, M.P. Bernquerer, D. Pilo-Veloso, A.P. Valente, F.C.L. Almeida, B. Bechinger, Structure and membrane interactions of the antibiotic peptide Dermadistinctin K by multidimensional solution and oriented N-15 and P-31 solid-state NMR spectroscopy, Biophys. J. 96 (2009) 2194–2203.
[47] D.K. Chang, S.F. Cheng, V.D. Trivedi, S.H. Yang, The amino-terminal region of the fusion peptide of influenza virus hemagglutinin HA2 inserts into sodium dodecyl sulfate micelle with residues 16-18 at the aqueous boundary at acidic pH - oligomerization and the conformational flexibility, J. Biol. Chem., 275 (2000) 19150–19158.
[48] C. Gray, S.A. Tatulian, S.A. Wharton, L.K. Tamm, Effect of the N-terminal glycine on the secondary structure, orientation, and interaction of the influenza hemagglutinin fusion peptide with lipid bilayers, Biophys. J. 70 (1996) 2275–2286.
[49] A.L. Lai, H. Park, J.M. White, L.K. Tamm, Fusion peptide of influenza hemagglutinin requires a fixed angle boomerang structure for activity, J. Biol. Chem. 281 (2006) 5760–5770.
[50] Z. Zhou, J.C. Macosko, D.W. Hughes, B.G. Sayer, J. Hawes, R.M. Epand, N-15 NMR study of the ionization properties of the influenza virus fusion peptide in zwitterionic phospholipid dispersions, Biophys. J. 78 (2000) 2418–2425.
[51] B. Bechinger, C. Aisenbrey, The polymorphic nature of membrane-active peptides from biophysical and structural investigations, Current Protein and Peptide Science 13 (2012) 602–610.
[52] J.M. Resende, R.M. Verly, C. Aisenbrey, A. Cesar, P. Bertani, D. Piló-Veloso, B. Bechinger, Membrane interactions of phylloseptin-1,-2, and-3 peptides by oriented solid-state NMR spectroscopy, Biophys. J. 107 (2014) 901–911.
[53] V.R. Kodati, R. Eljastimi, M. Lafleur, Contribution of the intermolecular coupling and librotorsional mobility in the methylene stretching modes in the infrared spectra of acyl chains, J. Phys. Chem. 98 (1994) 12191–12197.
[54] C.H. Chen, J.P. Ulmschneider, M.B. Ulmschneider, Mechanisms of a small membrane-active antimicrobial peptide from Hyla punctata, Aust. J. Chem. 73 (2020) 236–245.
[55] E.J. Dufourc, S. Buchoux, J. Toupe, M.A. Sani, F. Jean-Francois, L. Khemtemourian, A. Grelard, C. Loudet-Courreges, M. Laguerre, J. Elezgaray, B. Desbat, B. Odaert, Membrane interacting peptides: from killers to helpers, Curr. Protein Pept. Sci. 13 (2012) 620–631.
[56] A. Marquette, B. Bechinger, Biophysical investigations elucidating the mechanisms of action of antimicrobial peptides and their synergism, Biomolecules 8 (2018).
[57] A. Hagarman, T. Measey, R.S. Doddasomayajula, I. Dragomir, F. Eker, K. Griebenow, R. Schweitzer-Stenner, Conformational analysis of XA and AX dipeptides in water by electronic circular dichroism and H-1 NMR spectroscopy, J. Phys. Chem. B 110 (2006) 6979–6986.
[58] M.M. Domingues, M. Castanho, N.C. Santos, rBPI(21) promotes lipopolysaccharide aggregation and exerts its antimicrobial effects by (hemi)fusion of PG-containing membranes, PLoS One 4 (2009).
[59] A. Zemel, D.R. Fattal, A. Ben-Shaul, Energetics and self-assembly of amphipathic peptide pores in lipid membranes, Biophys. J. 84 (2003) 2242–2255.